Synthesis of tin nanoparticles on Ketjen Black in ionic liquid and water for the hydrogen evolution reaction

Lars Rademacher[1], Thi Hai Yen Beglau[1], Özgür Karakas[1], Alex Spieß[1], Dennis Woschko[1], Tobias Heinen[1], Juri Barthel[2] and Christoph Janiak*[1]

Address:

[1]Institut für Anorganische Chemie und Strukturchemie, Heinrich-Heine-Universität Düsseldorf, 40204 Düsseldorf, Germany,

[2]Ernst Ruska-Zentrum für Mikroskopie und Spektroskopie mit Elektronen, Forschungszentrum Jülich GmbH, 52425 Jülich, Germany

E-Mail:

Christoph Janiak - janiak@uni-duesseldorf.de*

** Corresponding author, Tel: +49-211-81-12286*

Keywords:

tin nanoparticles, ionic liquid, Ketjen Black, electrocatalysis, hydrogen evolution reaction

Abstract

Tin nanoparticles (Sn-NPs) embedded in Ketjen Black carbon (KB) were synthesized from anhydrous tin(II) chloride by reduction with sodium borohydride in the presence of different imidazolium based ionic liquids (ILs) or water and tested towards the hydrogen evolution reaction (HER) in electrocatalytic water splitting. Transmission and scanning electron microscopy showed the formation of well distributed Sn-NPs on KB with average sizes of 49 ± 25 to 96 ± 49 nm depending on the IL or water medium. Porosity was investigated by nitrogen sorption measurements indicating the preservation of the mesoporous structure of KB with BET surface areas in the range of 276 to 568 $m^2\ g^{-1}$ and total pore volumes of 0.38 to 0.75 $cm^3\ g^{-1}$. The metal content of the Sn/KB composites was determined by thermogravimetric analysis to be between 31 to 46 wt%. Sn/KB synthesized in HCl/H_2O showed a better performance towards HER with an overpotential of 136 mV compared to the overpotential of the other samples synthesized in IL ranging between 205 and 319 mV. Tafel analysis yielded a slope of 120 mV/dec and a low charge transfer resistance confirmed the good performance of Sn/KB synthesized in HCl/H_2O. After stability test the sample synthesized in the IL [HO-EMIm][BF_4] demonstrated an improved performance with an overpotential of 166 mV.

1. Introduction

Considering the growing need for energy storage for the increasing implementation of renewable energies, electrocatalytic produced hydrogen is a promising candidate not only for many energy demanding applications but also for the chemical industry as feedstock and even for steel production.[1,2,3] Often expensive metals like platinum are used as electrocatalysts for the hydrogen evolution reaction in water splitting.[4] However, there is a great interest in finding non-precious metals with high electrocatalytic activity, which comprises a low overpotential, a high stability, fast kinetics and low costs.[5,6,7,8]

Tin based materials are promising candidates due to their activity towards the hydrogen evolution reaction (HER) and lower costs compared to noble metals like platinum.[9] Tin compounds are already used in electrochemical applications for lithium batteries[10], for the electrocatalytic reduction of carbon dioxide[11] and for supercapacitors.[12,13] To the best of our knowledge, only few studies of Sn-based materials for HER, especially regarding monometallic materials, have been done. Ola et al. for example synthesized different Sn nanostructures on graphitic carbon nitride with sizes up to 4.5 µm by chemical vapor deposition and overpotentials starting at 260 mV.[14] Zhang et al. tested different tin oxide nanostructures delivering overpotentials starting at approximately 148 mV.[15] Shinde et al. used tin(II) sulfide nanoparticles (NPs) on nitrogen reduced graphene and achieved an overpotential of 125 mV[16]. Ravula et al. synthesized and tested tin disulfide forming plate like and nanoparticular structures on reduced graphene oxide whose overpotentials exceeded 500 mV.[17] Azizi et al. investigated the electrocatalytic properties of metallic Sn bars and showed that the Tafel slope reaches a value of 126 mV dec^{-1} indicating the Volmer reaction as rate determining step.[18]

Nanostructures provide a high surface area and thereby allow for a high activity but stabilizers are needed to prevent the thermodynamically favored agglomeration. Ionic liquids (ILs) can act as molecular stabilizer with adjustable properties.[19, 20] Several studies deal with the use of ILs for electrocatalytic applications. Zhang et al. achieved very low overpotentials starting at 169 mV by molybdenum dioxide particles synthesized in [BMIm][NTf_2].[21] Siebels et al. synthesized rhodium and platinum NPs supported on a covalent triazine-based framework by a simple microwave reaction in [BMIm][NTf_2], which then showed a low overpotential of 77 mV and a Tafel slope of 37 mV dec^{-1} towards HER.[22] In these cases, ILs exhibited outstanding stabilizing properties corresponding to weak coordinating cations and anions preventing the thermodynamically favored agglomeration of NPs.[19,20]

Here we tested Sn-NPs for the first time embedded in KB and synthesized in ILs towards HER. The Sn/KB composites were synthesized by a simple chemical reduction reaction and the medium IL was compared to HCl/H_2O as solvent to try to provide an alternative to noble metal containing materials, which are typically used as electrocatalysts for HER.

2. Experimental

2.1 Materials

$SnCl_2$ (98 %) was obtained from Across Organics, Ketjen Black EC 600JD from Akzo Nobel and $NaBH_4$ (for synthesis) from AppliChem. For the synthesis of [BMIm][Cl] 1-chlorobutane (>99 %) from Alfa Aesar and N-methylimidazole (>99 %) from Tokyo Chemical Industries was used. $LiNTf_2$ from Fluorochem, HPF_6 (60 wt.% in H_2O) from Sigma Aldrich and HBF_4 (50 wt.% in H_2O) from Alfa Aesar were employed for the chloride to NTf_2^-, PF_6^- or BF_4^- ion exchange to yield the ILs. [HO-EMIm][BF_4] was purchased from io-li-tec and used as received. Pt/C (20 wt.%) was obtained from Sigma Aldrich. [BMIm][NTf_2], [BMIm][PF_6] and [BMIm][BF_4] were synthesized by first reacting 1-chlorobutane with 1-methylimidazole to yield [BMIm][Cl].[23] Subsequently, the ion exchange was carried out with $LiNTf_2$, HPF_6 or HBF_4.[24] Impurities were removed with active carbon and by washing with water. Afterwards the ILs were pre-dried under vacuum at 70 °C for 5 h and further under high vacuum (<10^{-6} mbar) for 5 h. The purity was confirmed with ^{1}H-/^{13}C-NMR and anion chromatography to over 98 %. The water content was determined twice by Karl-Fisher titration to less than 10 ppm for [BMIm][NTf_2], [BMIm][PF_6], to ~500 ppm for [BMIm][BF_4] and to ~16.000 ppm for [HO-EMIm][BF_4].

2.2 Synthesis of Sn/KB materials

For the synthesis of Sn/KB 31.6 mg (0.167 mmol) of anhydrous $SnCl_2$ and 20 mg of KB were dispersed in 2 g of IL or N_2-saturated 0.1 mol L^{-1} HCl solution. Furthermore, 63.5 mg (1.667 mmol) of $NaBH_4$ was mixed with 2 g of the used IL or HCl medium. The $SnCl_2$ solutions and the $NaBH_4$/IL dispersions were stirred under inert atmosphere for 4 h and sonicated for 30 min. $NaBH_4$ in N_2-saturated 0.1 mol L^{-1} HCl solution was prepared directly before use. The corresponding solutions were combined and stirred for 24 h for samples prepared in IL and for 1 h for Sn/KB_H_2O to complete the reaction. The products were then handled in air. Samples prepared in IL were washed with acetonitrile and acetone (3 x 4 mL) with intermediate separation by centrifugation (6000 rpm) until a colorless and clean washing solution was obtained. The Sn/KB sample from HCl/H_2O was washed with acetone only. Products were dried under vacuum for 8 h and stored under inert (Ar) atmosphere. The samples were designated according to the used solvent as Sn/KB_IL or Sn/KB_H_2O.

2.3 Electrochemical measurements

For electrochemical measurements an Interface 1010E potentiostat from Gamry Instruments coupled with RRDE-3A station from ALS Japan was used consisting of a platinum wire, a Ag/AgCl reference electrode (with saturated 3.5 mol L^{-1} KCl solution) and a glassy carbon electrode (5 mm diameter). The catalyst loading was 0.255 mg cm^{-2}. A N_2-saturated 0.5 mol L^{-}

[1] H_2SO_4 solution serves as electrolyte. Potentials were converted to values with reference to reversible hydrogen electrode (RHE). HER measurements were conducted at different potentials and scan rates ranging from 0.1 to –0.8 V vs. RHE and 10 to 100 mV s^{-1} at a rotation rate of 3600 rpm. Prior to electrochemical measurements the samples were activated with several sweeps. The polarization curves were corrected by iR compensation. Electrochemical impedance spectroscopy (EIS) was performed at -290 mV vs. RHE in a frequency range of 1 to 100 kHz.

3. Results and Discussion

3.1 Synthesis and characterization of Sn-NPs on KB

The synthesis of metal NPs in ILs using a reduction agent is an established method.[19] The Sn/KB materials in this work were synthesized by chemical reduction of $SnCl_2$ with $NaBH_4$ in the presence of KB in different ILs or water under nitrogen atmosphere. From the used amount of $SnCl_2$ a Sn loading of 50 wt% could be theoretically achieved in every Sn/KB sample. Powder X-ray diffraction (PXRD) measurements show the presence of body-centered tetragonal (bct) Sn reproducibly in every sample (Fig. 1). The reflexes of the samples synthesized in IL have a wider full width at half maximum than the sample in HCl/water which translates into smaller crystallites for the former (Table 1). The crystallite sizes were calculated by the Scherrer equation (Eq. 1, SI) using the four strongest reflexes corresponding to (200), (101), (220) and (211) in the powder pattern (Tab. 1). The averaged crystallite sizes range between 22 to 38 nm. As expected, the crystallite size decreases with the use of ILs due to their stabilizing effect.

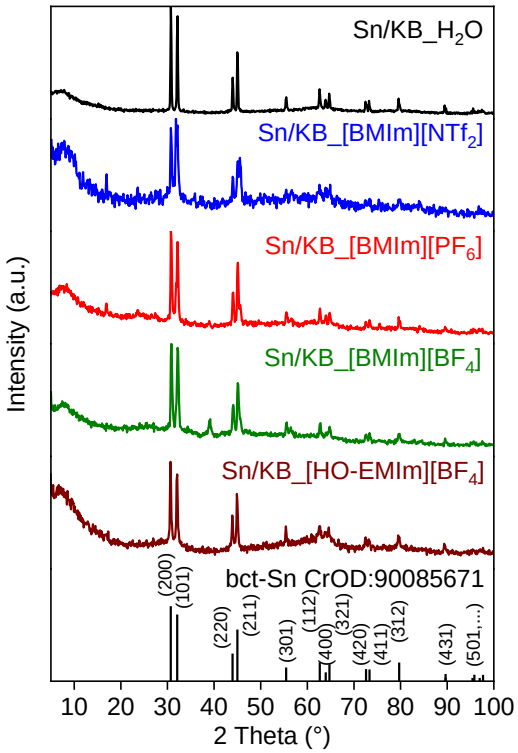

Fig. 1. PXRD patterns of Sn/KB materials synthesized in various ILs and in HCl/H_2O. The diffractogram of bct-Sn was simulated based on the crystallographic open database (CrOD 9008570) cif-file.

Table 1

NP sizes, crystallite sizes, Sn contents and results from nitrogen sorption experiments of the Sn/KB materials.

Sn/KB	NP size by TEM (nm) [a]	Crystallite size by PXRD (nm) [b]	Sn content by TGA (%)	BET surface area (m^2/g) [c]	Total pore volume (cm^3/g) [d]
_H_2O	49 ± 25	38 ± 2	46	479	0.64
_[BMIm][NTf_2]	54 ± 20	22 ± 2	42	276	0.38
_[BMIm][PF_6]	65 ± 25	27 ± 4	36	568	0.75
_[BMIm][BF_4]	96 ± 49	24 ± 2	45	378	0.52
_[HO-EMIm][BF_4]	49 ± 30	30 ± 3	31	452	0.67
KB alone	--	--	--	1385	1.84

[a] The size and size distribution was manually determined from 150 particles. [b] Calculated by the Scherrer equation using the first four reflexes at (200), (101), (220) and (211), Scherrer factor = 1. [c] Five adsorption points between p/p_0 = 0.1 – 0.3 were selected for BET determination. [d] Total pore volume at p/p_0 = 0.95.

Characterization towards morphology and size of the synthesized Sn/KB composites was done by transmission electron microscopy (TEM) which gave average Sn nanoparticle sizes from 50 to 100 nm (Fig. 2, Fig. SI1, Supporting Information (SI)), in good agreement with the expected smaller average crystallite size from the Scherrer equation (PXRD) which ranged from 22 to 38 nm. The crystallite size is usually smaller than the particle size when the latter are formed by aggregated crystallites. For estimation of the mean particle size, 150 particles were estimated and averaged (Tab. 1). The size distribution in the TEM images also shows diameters above 100 nm (Fig. 2). Within the series of samples Sn/KB_[BMIm][BF_4] exhibits the highest average particle size, indicating a weaker stabilization of the formed NP towards particle growth by the IL. Fig. 2a-e show the Sn particles which are surrounded by or deposited on KB particles. The Sn particles are faceted, indicative of nanocrystals, which cluster in aggregated structures (Fig. SI2). The KB shows only with low contrast against the carbon-coated copper grid. Representative selected area diffraction (SAED) (Fig. 2f) of the particles in Fig. 2a confirms the presence of bct-Sn due to strong diffraction spots belonging to the (200),

(101), (220) and (211) crystal planes. Energy-dispersive X-ray (EDX) spectra at the positions in Fig. 2 show the presence of Sn in each sample (Fig. SI1).

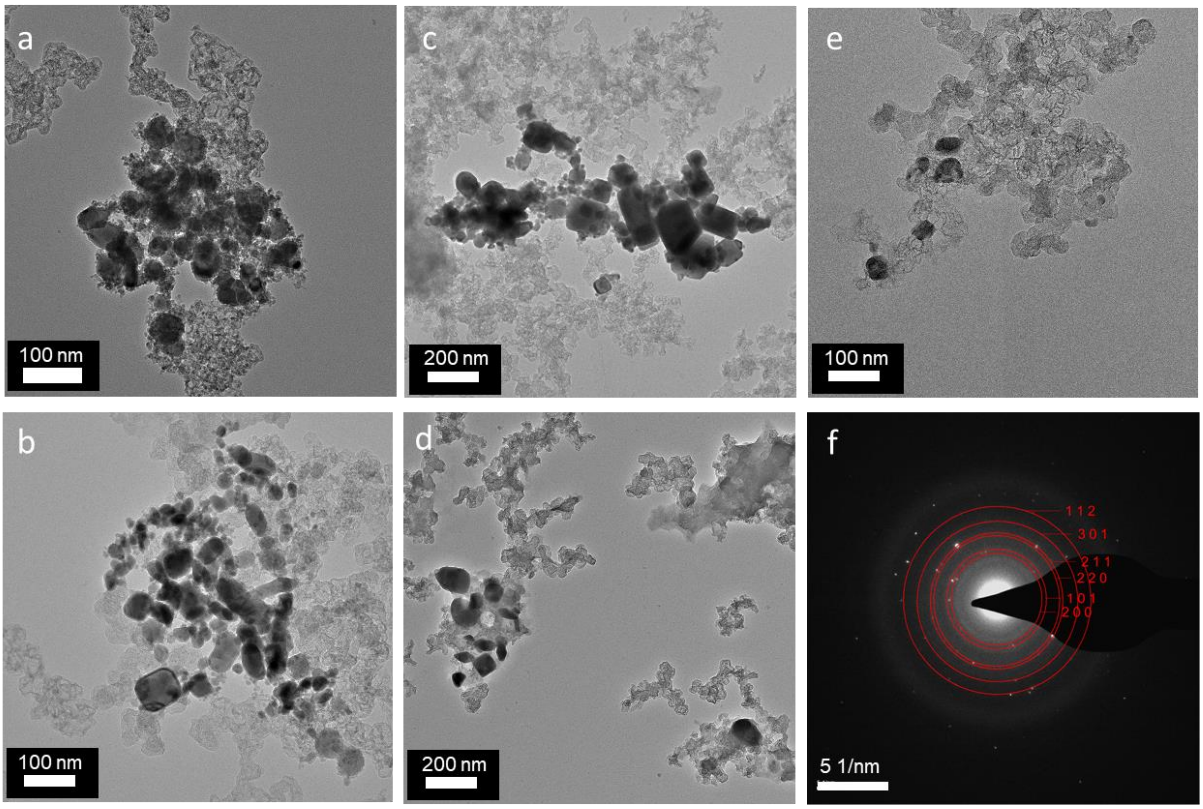

Fig. 2. TEM images of Sn/KB_H_2O (a), Sn/KB_[BMIm][NTf_2] (b), Sn/KB_[BMIm][PF_6] (c), Sn/KB_[BMIm][BF_4] (d) and Sn/KB_[HO-EMIm][BF_4] (e). SAED pattern of Sn/KB_H_2O (f).

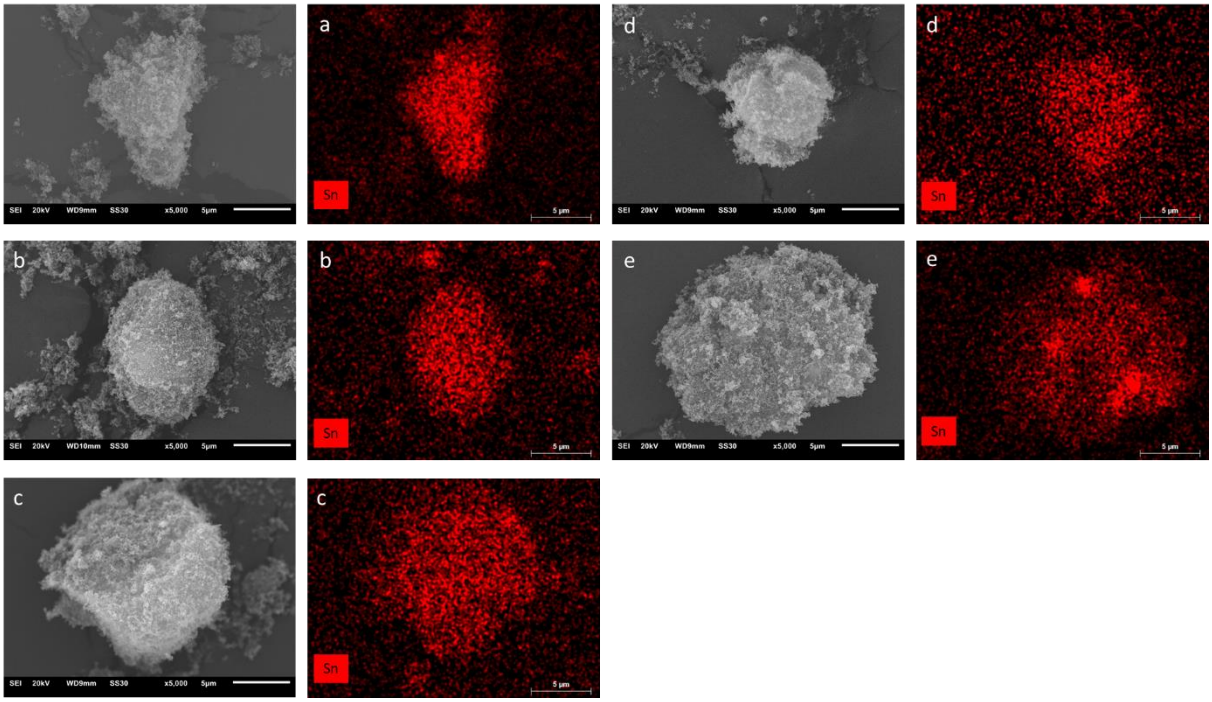

Fig. 3. SEM images and EDX elemental mappings of Sn (in red) for Sn/KB_H_2O (a), Sn/KB_[BMIm][NTf_2] (b), Sn/KB_[BMIm][PF_6] (c), Sn/KB_[BMIm][BF_4] (d) and Sn/KB_[HO-EMIm][BF_4] (e).

The distribution of Sn was further investigated by scanning electron microscopy (SEM) and SEM-EDX mapping (Fig. 3) and shows a rather uniform coverage of Sn on the surface of large KB agglomerates. X-ray photoelectron spectroscopy (XPS) studies confirmed the zero-valent oxidation state of Sn (Fig. SI3). All high-resolution Sn 3d spectra confirm Sn(0) with binding energies of 485.3 ± 2 eV for Sn $3d_{1/2}$ and 485.6 ± 2 eV for Sn $3d_{3/2}$ [25,26] and rule out any remaining Sn(II).

Sn loadings on KB were determined by thermogravimetric analysis (TGA) based on residual masses of SnO_2 assuming the complete oxidation of Sn(0) to SnO_2 (Tab. 1, Fig. SI5). The composite Sn/KB_[HO-EMIm][BF_4] had the lowest (31 wt%) and Sn/KB_H_2O together with Sn/KB_[BMIm][BF_4] had the highest Sn loading (46 wt%). Thus, it can be concluded that the synthesis in [BMIm][BF_4] and HCl/water results in better reduction to Sn(0) and subsequent deposition on KB.

Nitrogen sorption measurements of KB alone and the Sn/KB materials yielded type II adsorption isotherms with a type H3 hysteresis loop for desorption (Fig. 4), indicative of macroporous materials and non-rigid aggregates.[27] The porosity is due to KB which has a BET surface area S(BET) of 1385 $m^2\ g^{-1}$ and a total pore volume of 1.84 g cm^{-3}. Noteworthy, the BET surfaces areas for Sn/KB are significantly lower than the calculated values from the mass-weighted S(BET) of 1385 $m^2\ g^{-1}$ of KB according to Eq. 1. For a Sn content of 31 wt% as in Sn/KB_[HO-EMIM][BF_4] the expected S(BET) would be 956 $m^2\ g^{-1}$ whereas 452 $m^2\ g^{-1}$ were found. For a Sn content of 46 wt% as in Sn/KB_H_2O the S(BET) of 748 $m^2\ g^{-1}$ is calculated, while 479 $m^2\ g^{-1}$ were found.

$$S(BET)_{calc.} = \frac{\text{wt\% of KB}}{100} \times S(BET,KB) = \frac{100\text{-wt\% of Sn}}{100} \times S(BET,KB) \qquad (1)$$

The lower than expected surface areas and porosities of the Sn/KB composites may not be traced to residual IL, since the effect is also observed in Sn/KB_H_2O, but to pore-blocking and pore-filling by the formation of the Sn nanoparticles. Still some porosity remains in the composites which is essential for ion conductivity and mass transport during electrocatalysis.[5]

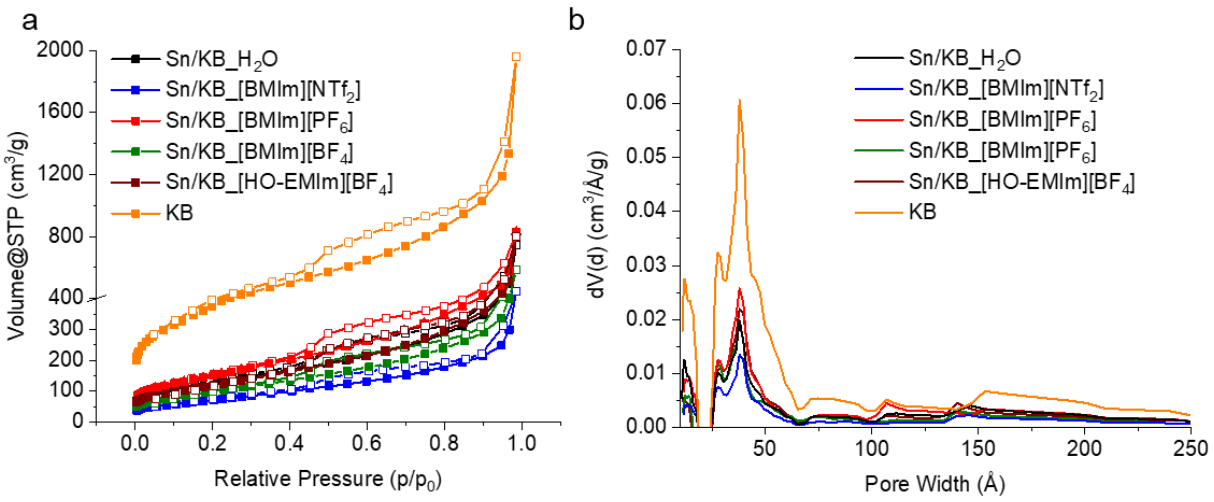

Fig. 4. Nitrogen sorption isotherms (a) (adsorption: filled boxes; desorption: empty boxes) and pore size distribution curves (b) of the Sn/KB materials.

3.2 Electrochemical properties

The electrocatalytic properties of the Sn/KB composites towards HER were measured twice, to ensure reproducibility, in a three-electrode setup in a 0.5 mol L^{-1} H_2SO_4 electrolyte and was compared to commercial 20 wt% Pt/C. Fig. 5a shows the polarization curves of the synthesized Sn/KB materials and Pt/C. It can be seen that the polarization curves of the samples synthesized in [HO-EMIm][BF_4] and in water are closest to the theoretical HER starting point at 0 V vs. RHE, while the polarization curves of Sn/KB_[BMIm][PF_6], Sn/KB_[BMIm][NTf_2] and Sn/KB_[BMIm][BF_4] are increasingly shifted to more negative potentials. Fig. 5b gives a graphical presentation of the overpotentials at 10 mA cm^{-2} taken from the polarization curves before and after stability test. At this current density Sn/KB_H_2O synthesized in water shows an overpotential of 137 mV vs. RHE while the samples which were synthesized in IL, require overpotentials above 200 mV to reach 10 mA cm^{-2} (Tab. 2). For comparison, the 20 wt% Pt/C standard has an overpotential of 46 mV at 10 mA cm^{-2}, which is in accordance with the literature.[9]

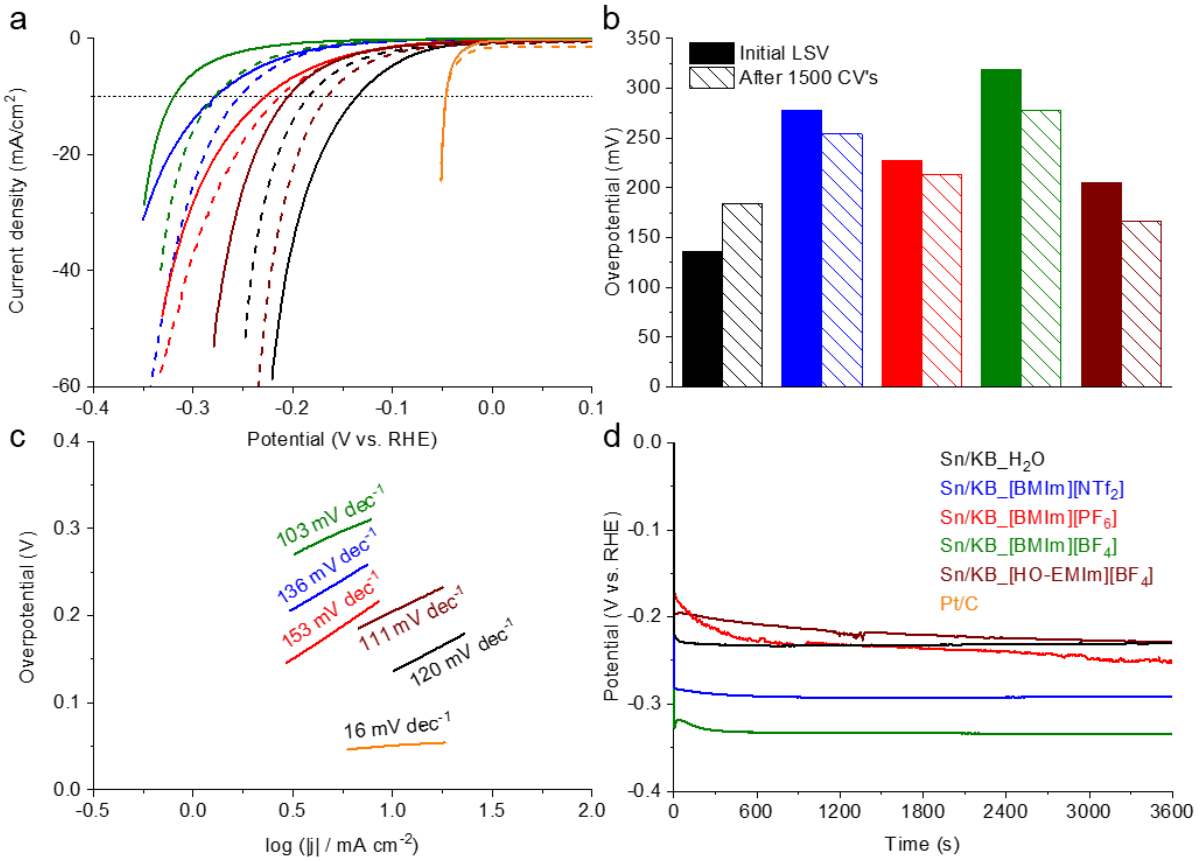

Fig. 5. HER polarization curves (a) (before stability test: solid lines; after stability test: dashed lines), overpotentials at 10 mA cm^{-2} (b), Tafel plots (c) and chronopotentiometry at 15 mA cm^{-2} (d) of the Sn/KB materials (Pt/C was not investigated by chronopotentiometry).

Tafel plots were made to evaluate the materials regarding reaction kinetics and the sensitivity of the current to a change in the applied potential (Fig. 5c). It should be noted that the kinetics of HER depend on the reaction path. Ideal catalysts should have low Tafel slopes besides low overpotentials.[5] As expected, the Pt/C standard shows a Tafel slope of only 16 mV dec^{-1}, which also indicates that the Tafel reaction 2 M-H* ⇆ 2 M + H_2 is the rate determining reaction.[9] The Tafel slopes of the Sn/KB materials are in a range of 103 to 153 mV dec^{-1} (Tab. 2) with the samples from the two BF_4 ILs Sn/KB_[BMIm][BF_4] and Sn/KB_[HO-EMIm][BF_4] have the lowest slopes (103 mV dec^{-1} and 111 mV dec^{-1}, respectively). The samples synthesized in the NTf_2 and PF_6 ILs gave the highest slopes with 136 mV dec^{-1} and 153 mV dec^{-1}. In general, the slopes for Sn/KB are relatively high in comparison to the measured overpotential and the Tafel slopes of other materials (Tab. SI1). Due to these high slope values of ~120 mV dec^{-1}, the Volmer reaction $H^+ + M + e^- ⇆$ M-H* can be assumed as rate determining step for these materials in the acidic electrolyte.[5]

For evaluating the electrochemical stability of the Sn/KB materials, durability tests with cyclic potentials sweeps (CV) were conducted. From Fig. 5b it can be seen that the sample synthesized in water shows an increase in the overpotential from 136 to 184 mV after 1500

cycles, corresponding to deactivation. The other samples exhibit an activation, that is lower overpotentials after the stability test. Pt/C remains unchanged. In particular the overpotential of Sn/KB_[HO-EMIm][BF_4] drops to 166 mV upon activation. Even after 1500 cycles the overpotentials of the other Sn/KB_IL samples stay above 200 mV (at 10 mA cm^{-2}). To check the stability at a constant current, chronopotentiometry at 15 mA cm^{-2} was carried out after 1500 CVs and shows stable potentials during 1 h at constant current (Fig. 5d). For Sn/KB_[BMIm][PF_6] and Sn/KB_[HO-EMIm][BF_4] a slightly decreasing performance can be observed which the other Sn/KB samples are stable. Another durability test of Sn/KB_[HO-EMIm][BF_4] confirms the good long-term performance during 16 h chronopotentiometry (Fig. SI6).

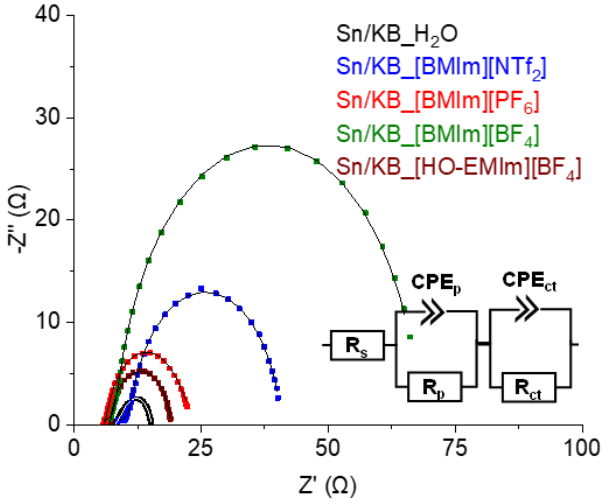

Fig. 6. Nyquist plot of Sn/KB materials at -290 mV vs. RHE. Data are fitted to a Voigt circuit model (solid lines) with resistance elements for the electrolyte R_s, electrode porosity R_p and charge transfer R_{ct}. Double-layer capacitance is represented by constant phase elements CPE.[28,29]

Furthermore, electrochemical impedance spectroscopy (EIS) was conducted before the stability test to evaluate the impedance of the materials at a defined alternating current (AC) potential. Fig. 6 shows the resulting Nyquist plots of the Sn/KB materials at a potential of –290 mV vs. RHE. From the shape of the semicircles it can be seen that the samples continue to follow the similar trend as in the previous electrochemical results. Sn/KB_H_2O shows the Nyquist plot with the smallest radius at this AC potential indicating the best performance in the series due to a low charge transfer resistance. To estimate specific values for the charge transfer resistances, a Voigt circuit model was fitted to the experimental data. The values confirm the above conclusions and give the lowest charge transfer resistance with 3.0 Ω for Sn/KB_H_2O followed by Sn/KB_[HO-EMIm][BF_4] with 11.1 Ω indicating a slower electron transfer (Tab. 2).

Table 2

Overpotentials at 10 mA cm^{-2}, Tafel slopes and estimated charge transfer resistances of the Sn/KB materials at -290 mV vs. RHE.

Sn/KB	**Overpotential at 10 mA cm^{-2} (mV) [a]**	**Tafel slope (mV dec^{-1})**	**Charge transfer resistance (Ω) [b]**	**Overpotential after 1500 CVs at 10 mA cm^{-2} (mV)**
_H_2O	137	120	3.0	184
_[BMIm][NTf_2]	278	136	23.4	254
_[BMIm][PF_6]	228	153	11.5	213
_[BMIm][BF_4]	319	103	71.8	278
_[HO-EMIm][BF_4]	205	111	11.1	166

[a] See Table SI1 for further comparisons to other materials. [b] Evaluation by using a Voigt circuit model for data fitting.[30]

4. Conclusion

Sn/KB composite materials were synthesized using imidazolium-based ILs or acidic water (hydrochloric acid) as solvents and were tested towards the HER. The formation of metallic Sn nanoparticles was confirmed by PXRD, TEM- and SEM-EDX as well as XPS. Larger Sn-NPs were observed when IL was used. Nitrogen sorption showed reduced BET surfaces and pore volumes except for the sample synthesized in [BMIm][PF_6] having a much lower Sn content. Sn/KB synthesized from hydrochloric acid, Sn/KB_H_2O showed the best performance with a low overpotential of 137 mV to reach 10 mA cm^{-2}, a Tafel slope of 120 mV dec^{-1} and a low charge transfer resistance, while materials synthesized in ILs gave higher overpotentials. Yet, after the stability test the overpotential increased to 184 mV for Sn/KB_H_2O. To the contrary, a small activation is present in stability tests with the samples prepared in ILs. Thereby, the overpotential for Sn/KB_[HO-EMIm][BF_4] becomes lower (166 mV) than for Sn/KB_H_2O (184 mV) after the stability tests. Also, the other IL samples improved their overpotential after the stability test. A reason for these phenomena could be the strong interaction of IL with the surface of KB or the Sn-NPs. It can be assumed that IL remains on the surface of the particles reducing the initial electrocatalytic activity but preventing the NPs from aggregation. Partial removal of the IL during the time of the stability test then sets additional Sn surface free for the improved performance. Still, the interaction of a metal NP with IL is far from understood.[20] In contrast to other monometallic Sn-based materials, we obtained Sn particles with sizes on the nanoscale, embedded in or deposited on Ketjen Black, by a simple chemical reduction using $NaBH_4$ and different solvents, demonstrating remarkable performances towards HER.

CRediT authorship contribution statement

Lars Rademacher: Conceptualization, Methodology, Formal analysis, Investigation, Visualization, Writing – original draft, Writing – review & editing. **Thi Hai Yen Beglau:** Investigation, Formal analysis **Özgür Karakas:** Investigation, Formal analysis **Alex Spieß**: Investigation. **Dennis Woschko:** Investigation. **Tobias Heinen:** Investigation. **Juri Barthel:** Resources. **Christoph Janiak:** Resources, Supervision, Funding acquisition, Writing – review & editing

Declaration of Competing Interest

The authors declare that they have no known competing financial interest or personal relationships that could have appeared to influence the work reported in this paper

References

1 P. P. Edwards, V. L. Kuznetsov, W. I. F. David, *Philos. Trans. A. Math. Phys. Eng. Sci.* **2007**, 365, 1043-1056. https://doi.org/10.1098/rsta.2006.1965

2 N. Rambhujun, M. S. Salman, T. Wang, C. Pratthana, P. Sapkota, M. Costalin, Q. Lai, K.-F. Aguey-Zinsou, *MRS Energy & Sustainability* **2020**, 7, 1-16. https://doi.org/10.1557/mre.2020.3

3 J. Gretz, W. Korf, R. Lyons, *Int. J. Hydrog. Energy* **1991**, 16, 691-693. https://doi.org/10.1016/0360-3199(91)90193-M

4 S. Ravula, C. Zhang, J. B. Essner, J. D. Robertson, J. Lin, G. A. Baker, *ACS Appl. Mater. Interfaces* **2017**, *9*, 8065-8074. https://doi.org/10.1021/acsami.6b13578

5 M. Zeng, Y. Li, *J. Mater. Chem. A* **2015**, 3, 14942-14962. https://doi.org/10.1039/C5TA02974K

6 J. Ying, X. Y. Yang, G. Tian, C. Janiak, B. L. Su, *Nanoscale* **2014**, 6, 13370-13382. https://doi.org/10.1039/C4NR03225J

7 S. Gong, Y.-X. Zhang, Z. Niu, *ACS Catal.* **2020**, 10, 10886-10904. https://doi.org/10.1021/acscatal.0c02587

8 Y. Xin, S. Li, Y. Qian, W. Zhu, H. Yuan, P. Jiang, R. Guo, L. Wang, *ACS Catal.* **2020**, 10, 11280-11306. https://doi.org/10.1021/acscatal.0c03617

9 O. Ola, Y. Chen, K. Thummavichai, Y. Zhu, *Sustain. Energy Fuels* **2020**, 4, 5223-5228. https://doi.org/10.1039/D0SE00812E

10 N. Soulmi, D. Dambournet, C. Rizzi, J. Sirieix-Plénet, M. Duttine, A. Wattiaux, J. Swiatowska, O. J. Borkiewicz, H. Groult, L. Gaillon, *Inorg. Chem.* **2017**, 56, 10099-10106. https://doi.org/10.1021/acs.inorgchem.7b01850

11 J. Gu, F. Héroguel, J. Luterbacher, X. Hu, *Angew. Chem. Int. Ed.* **2018**, 57, 2943-2947. https://doi.org/10.1002/anie.201713003

12 Y. Zhao, J. Liang, C. Wang, J. Ma, G. G. Wallace, *Adv. Energy Mater.* **2018**, 8, 1702524-1702524. https://doi.org/10.1002/aenm.201702524

13 V. Velmurugan, U. Srinivasarao, R. Ramachandran, M. Saranya, A. N. Grace, *Mater. Res. Bull.* **2016**, 84, 145-151. https://doi.org/10.1016/j.materresbull.2016.07.015

14 O. Ola, Y. Chen, K. Thummavichai, Y. Zhu, *Sustain. Energy Fuels* **2020**, 4, 5223-5228. https://doi.org/10.1039/D0SE00812E

15 Y. Zhang, J. Zou, Z. He, Y. Zhao, X. Kang, Y. Zhao, Z. Miao, *J. Alloy. Compd.* **2021**, 865, 158597. https://doi.org/10.1016/j.jallcom.2021.158597

16 S. S. Shinde, A. Sami, D.-H. Kim, J.-H. Lee, *Chem. Commun.* **2015**, 51, 15716-15719. https://doi.org/10.1039/C5CC05644F
17 S. Ravula, C. Zhang, J. B. Essner, J. D. Robertson, J. Lin, G. A. Baker, *ACS Appl. Mater. Interfaces* **2017**, 9, 8065-8074. https://doi.org/10.1021/acsami.6b13578
18 O. Azizi, M. Jafarian, F. Global, H. Heli, M. Mahjan, *Int. J. Hydrog. Energy* **2007**, 32, 1755-1761. https://doi.org/10.1016/j.ijhydene.2006.08.043
19 C. Janiak, *Zeitschrift für Naturforschung B* **2013**, 68, 1059-1089. https://doi.org/10.5560/znb.2013-3140
20 S. Wegner, C. Janiak, Metal Nanoparticles, in: Ionic Liquids, B. Kirchner, E. Perlt. (eds) Ionic Liquids II. Topics in Current Chemistry Collections, Springer Berlin Heidelberg, **2017**, 153-184. https://doi.org/10.1007/978-3-319-89794-3_6
21 B. Zhang, Y. Xue, A. Jiang, Z. Xue, Z. Li, J. Hao, *ACS Appl. Mater. Interfaces* **2017**, *9*, 7217-7223. https://doi.org/10.1021/acsami.7b00722
22 M. Siebels, C. Schlüsener, J. Thomas, Y.-X. Xiao, X.-Y. Yang, C. Janiak, *J. Mater. Chem. A* **2019**, *7*, 11934-11943. https://doi.org/10.1039/C8TA12353E
23 A. Aupoix, B. Pégot, G. Vo-Thanh, *Tetrahedron* **2010**, 66, 1352-1356. https://doi.org/10.1016/j.tet.2009.11.110
24 P. Wasserscheid, T. Welton, Ionic Liquids in Synthesis, Wiley-VCH, Wannheim, 2007. https://doi.org/10.1002/9783527621194
25 Y. Okamoto, W. Carter, D. Hercules, *Appl. Spectrosc.* **1979**, 33, 287-293. https://doi.org/10.1366/0003702794925859
26 O. Ola, Y. Chen, K. Thummavichai, Y. Zhu, *Sustain. Energy Fuels* **2020**, 4, 5223-5228. https://doi.org/10.1039/D0SE00812E
27 M. Thommes, K. Kaneko, A.V. Neimark, J.P. Olivier, F. Rodriguez-Reinoso, J. Rouquerol, K.S.W. Sing, *Pure Appl. Chem.* **2015**, 87, 1051-1069. https://doi.org/10.1515/pac-2014-1117
28 Z. Shi, Y. Wang, H. Lin, H. Zhang, M. Shen, S. Xie, Y.Zhang, Q. Gao, Y. Tang, *J. Mater. Chem.* **2016**, 4, 6006-6013. https://doi.org/10.1039/C6TA01900E
29 A. K. Ipadeola, K. I. Ozoemena, RSC Adv. **2020**, 10, 17359-17368. https://doi.org/10.1039/D0RA02307H